Published in final edited form as:

Nature. 2015 June 4; 522(7554): 111–114. doi:10.1038/nature14267.

eIF3 targets cell proliferation mRNAs for translational activation or repression

Amy S.Y. Lee[1,2], **Philip J. Kranzusch**[1,3], and **Jamie H.D. Cate**[*,1,2,4,5]

[1]Department of Molecular & Cell Biology, University of California, Berkeley, Berkeley, CA 94720, USA

[2]Center for RNA Systems Biology, University of California, Berkeley, Berkeley, CA 94720, USA

[3]Howard Hughes Medical Institute (HHMI), University of California, Berkeley, Berkeley, CA 94720, USA

[4]Department of Chemistry, University of California, Berkeley, Berkeley, CA 94720, USA

[5]Physical Biosciences Division, Lawrence Berkeley National Laboratory, Berkeley, CA 94720, USA

Abstract

Regulation of protein synthesis is fundamental for all aspects of eukaryotic biology by controlling development, homeostasis, and stress responses[1,2]. The 13-subunit, 800-kDa eukaryotic initiation factor 3 (eIF3) organizes initiation factor and ribosome interactions required for productive translation[3]. However, current understanding of eIF3 function does not explain genetic evidence correlating eIF3 deregulation with tissue-specific cancers and developmental defects[4]. Here we report the genome-wide discovery of human transcripts that interact with eIF3 using photo-activatable crosslinking and immunoprecipitation (PAR-CLIP)[5]. eIF3 binds to a highly specific programme of messenger RNAs (mRNAs) involved in cell growth control processes, including cell cycling, differentiation, and apoptosis, via the mRNA 5′ untranslated region (5′ UTR). Surprisingly, functional analysis of the interaction between eIF3 and two mRNAs encoding cell proliferation regulators, c-Jun and BTG1, reveals that eIF3 employs different modes of RNA stem loop binding to exert either translational activation or repression. Our findings illuminate a new role for eIF3 in governing a specialized repertoire of gene expression and suggest that binding of eIF3 to specific mRNAs could be targeted to control carcinogenesis.

Extensive genetic evidence implicates eIF3 in other functions in translation outside of its general role as a protein scaffold for formation of initiation complexes. Mutation or inactivation of eIF3 subunits results in developmental defects in *C. elegans* and zebrafish[6,7].

*Correspondence to: jcate@lbl.gov, (510) 666-2749.

Author Contributions: Experiments were designed by A.S.Y.L. in consultation with J.H.D.C. All experiments and analyses were performed by A.S.Y.L. P.J.K performed gel shift assays and assisted with biochemistry. The manuscript was written by A.S.Y.L and J.H.D.C. All authors contributed to editing the manuscript and support the conclusions.

All data are deposited in Gene Expression Omnibus (accession number GSE65004).

The authors declare no competing financial interests.

Furthermore, analyses of human tumors reveals that overexpression of eIF3 is linked to diverse cancers, including breast, prostate, and esophageal malignancies[4,8]. The integral role of eIF3 during cellular differentiation, growth, and carcinogenesis, suggests eIF3 might drive specialized translation. Consistent with this hypothesis, translation of the hepatitis C virus RNA occurs through essential interactions between eIF3 and a structured Internal Ribosome Entry Site (IRES) element in the viral genome, indicating the feasibility of translation regulation being driven by distinct cellular eIF3–mRNA contacts[9].

To identify candidate transcripts regulated through direct interactions with eIF3, we first used a genome-wide approach to determine the eIF3 RNA binding targets in human 293T cells. Because eIF3 is composed of 13 subunits (eIF3a–m), we adapted a 4-thiouridine photoactivatable ribonucleoside-enhanced crosslinking and immunoprecipitation (PAR-CLIP)[5] approach to allow analysis of a large multimeric complex, with isolation of individual subunit-RNA libraries (Fig. 1a). As overexpression of single eIF3 subunits can alter complex assembly[8], we optimized immunoprecipitation of the full endogenous eIF3 complex using an antibody that recognizes the eIF3b subunit (Fig. 1b). High salt washes were used to ensure removal of potentially contaminating translation factors, such as eIF4G or the small ribosomal subunit (Fig. 1c). After RNase digestion, separation of crosslinked eIF3–RNA complexes by denaturing gel electrophoresis demonstrated that four of the thirteen subunits crosslink directly to RNA (Fig. 1d), identified by mass spectrometry as eIF3a, b, d, and g (Extended Data Fig. 1).

For each subunit, separate cDNA libraries were generated from the isolated crosslinked RNAs and deep sequenced using Illumina technology. Sequenced reads from three biological replicates were mapped to the genome and grouped into eIF3-binding sites by using the cluster-finding tool Paralyzer[10]. Read clusters were found in 479 unique genes, with eIF3a, b, d, and g crosslinking to 328, 264, 356, and 352 transcripts, respectively (Supplementary Table 1, 2). The limited number of interacting genes supports capture of specific eIF3–RNA contacts, as these targets compromise only ∼3% of total expressed transcripts (Extended Data Figure 2). As a further control, we do not see crosslinking to highly abundant rRNAs, in agreement with biochemical and structural studies showing that eIF3 interacts primarily with the protein-rich face of the small ribosomal subunit[11-14].

The majority of RNAs contained a single eIF3-binding site, with a median cluster length of 25 nt (Fig. 2a, b). These RNAs interact with distinct combinations of eIF3a, b, d, and g subunits (Fig. 2c). To validate the RNAs identified by PAR-CLIP, we performed eIF3 immunoprecipitation in the absence of crosslinking. We detected eIF3–RNA interactions for five top candidate genes using RT-PCR; whereas a negative control mRNA, the PSMB6 transcript, was not immunoprecipitated (Fig. 2d).

In eukaryotic protein synthesis, the 5′ UTR of mRNA is thought to be the major site of translation regulation[3]. In agreement with identifying translation regulation roles of specific eIF3–mRNA interactions, the eIF3 binding sites predominantly mapped to the 5′ UTR (∼70%) (Fig. 2e). To examine the impact of transcript-specific engagement of eIF3 on translational control, we focused on two genes with an eIF3 binding site in the 5′ UTR, *c-Jun* and *B cell translocation gene 1* (*BTG1*) (Fig. 3a, b). c-Jun is a member of the immediate

early response transcription factor AP1 and a positive mitotic regulator[15]. In contrast, BTG1 acts as a negative regulator of proliferation and its expression induces cellular differentiation[16,17]. Because of the opposing effects of c-Jun and BTG1 on cellular growth, we wanted to understand why eIF3 would interact with both mRNAs. We constructed luciferase reporters containing the 5′ UTR of c-Jun or BTG1 with or without the eIF3 crosslinking site identified by PAR-CLIP (Fig. 3c). Deletion of the crosslinking site from the 5′ UTR of c-Jun abolished translation of mRNAs transfected into cells, indicating that eIF3 binding is required for efficient translation (Fig. 3d). In stark contrast, BTG1 translation was highly up-regulated when the eIF3 binding site was removed from the mRNA (Fig. 3e). Furthermore, treatment of 293T *in vitro* translation extracts with m^7G cap analog inhibited translation of both c-Jun and BTG1 luciferase reporter mRNAs, demonstrating that eIF3-dependent translation regulation of these transcripts is cap-dependent and thus distinct from viral IRES-like mechanisms[18] (Fig. 3f, g). These results demonstrate that eIF3 can act as both a translation activator and repressor of specific cellular mRNAs.

To understand how eIF3 binding to mRNA leads to opposing translation phenotypes, we next identified the full RNA elements for eIF3 recognition in the c-Jun and BTG1 mRNAs. While PAR-CLIP marks the localized vicinity of eIF3 in the 5′ UTR, eIF3 interaction could occur either through recognition of a linear sequence or in the context of RNA secondary structure. Using selective 2′ hydroxyl acylation analyzed by primer extension (SHAPE), we experimentally determined the secondary structure around the eIF3 binding sites (Fig. 4a, d). For both c-Jun and BTG1, SHAPE revealed that the eIF3 binding sites map to structured RNA regions corresponding to conserved stem loops (Extended Data Fig. 3). For the c-Jun mRNA element, we investigated the importance of secondary structure in eIF3 recognition by mutating base-pairing interactions of five nucleotides in the stem while leaving the crosslinking site intact (Fig. 4b). eIF3 directly bound to the c-Jun stem loop, but not the mutated stem loop, as determined by native agarose gel electrophoresis with radiolabeled RNA and recombinant or native eIF3 (Fig. 4b, Extended Data Fig. 4). Furthermore, the same mutations in the c-Jun luciferase reporter mRNA led to the identical translation phenotype as deletion of the full eIF3 crosslinking site (Fig. 4c, Extended Data Fig. 5a). Unlike its interactions with the c-Jun RNA, eIF3 was unable to bind to the BTG1 stem loop in a binary fashion (Extended Data Fig. 4b). As eIF3 immunoprecipitates BTG1 mRNA in cell lysates (Fig. 2d), this suggests other currently unknown factors are required for this mode of eIF3–RNA interaction. To verify that the BTG1 stem loop is sufficient for the inhibitory translation phenotype of eIF3 binding, we asked if addition of the stem loop could block translation driven by the PSMB6 5′ UTR, which does not interact with eIF3 (Fig. 2d). Transplantation of the BTG1 stem loop into the PSMB6 5′ UTR conferred translation inhibition (Fig. 4e, Extended Data Fig. 5b). Importantly, addition of the transversed BTG1 stem loop sequence does not alter PSMB6 translation, confirming that BTG1 stem loop-driven translation repression is eIF3-specific and not due to introduction of a potentially deleterious RNA secondary structure[19] (Fig. 4e, Extended Data Fig. 5b). Together, these results demonstrate that during translation activation, eIF3 recognizes the c-Jun mRNA by directly binding to a sequence in the context of a stem loop structure; whereas during translation inhibition, eIF3 binding to the BTG1 stem loop requires the presence of additional factors or modifications.

Although misregulation of eIF3 levels is implicated in carcinogenesis, it was previously unknown if eIF3 activities lead to these cell growth alterations[4,8]. Gene ontology analysis of the PAR-CLIP results establish direct binding of eIF3 to RNA targets enriched in cancer-associated cell growth regulation pathways, such as apoptosis, cell cycling, and differentiation (Extended Data Fig. 6a). The combination of these targets likely represents a gene programme that supports overactive cell proliferation during eIF3-related malignancies. In support of this, our results demonstrate that eIF3 acts as a positive translational regulator of c-Jun, which is a proto-oncogene required for ras-mediated transformation[20]; and a negative regulator of BTG1, of which genomic deletions are found in 9% of B-cell precursor acute lymphoblastic leukemias[21]. Furthermore, circumventing eIF3 translational control by knockdown of c-Jun or overexpression of BTG1 decreases cell invasiveness of H1299 human lung cancer cells, which overexpress eIF3a[22] (Fig. 4f, g, Extended Data Fig. 6). Thus, we suggest that the RNAs identified by PAR-CLIP may be co-opted upon eIF3 overexpression, leading to loss of correct translational control of cell growth and eventual malignancy.

While it is surprising that eIF3 can act as both a repressor and activator of translation, analogous contrasting functions have been found with other multi-protein complexes. For example, the RNA polymerase II regulation complex, Mediator, consists of at least 30 proteins in humans. It directs either transcription activation or repression, dependent on promoter sequence, gene-specific regulatory proteins, and altered phosphorylation states of subunits[23]. Intriguingly, more than 25 post-translational modifications have been detected on eIF3, with a number of them at substoichiometric levels[24,25]; and eIF3 association with other translation regulatory proteins such as the helicase eIF4B is regulated by mitogenic signaling[26]. Furthermore, modeling of the eIF3 subunits, except for eIF3d, reveals that the crosslinked subunits form a nexus in a distal region of eIF3 positioned near the mRNA entry tunnel (Extended Data Fig. 7)[14]. As the PAR-CLIP sites exhibit all variations of interactions with the four eIF3 subunits (Fig. 2c), we propose there may be multiple modes of eIF3–RNA interactions driven by this region of eIF3[12,13].

Recent studies have highlighted that certain factors possess roles outside of their general functions in translation. For example, the ribosome mediates translational specificity during development and viral infection through the requirement for distinct ribosomal proteins[27,28]. During canonical translation, eIF3 acts as a protein scaffold for initiation complex assembly[3]. Our results now reveal a new paradigm for translational control, where in addition to this general function, eIF3 can act as both an activator and repressor of cap-dependent transcript-specific translation through direct binding to defined RNA structural elements.

Methods

Cells and transfections

Human 293T cells were maintained in DMEM (Invitrogen) with 10% FBS (Tissue Culture Biologicals). H1299 cells were maintained in RPMI-1640 ATCC-formulated (ATCC) with 10% FBS. IMR90 cells were maintained in Eagles MEM (ATCC) with 10% FBS. RNA transfections were performed using TransIT mRNA reagent (Mirius), with the following

modifications to the manufacturer's protocol. 24 h prior to transfection, 293T cells were seeded into opaque 96-wells to be at ~80% confluence at the time of transfection. For each well, 9 μl of pre-warmed OptiMEM (Invitrogen) was mixed with 90 ng of RNA, 0.27 μl of Boost reagent, and 0.27 μl of TransIT mRNA reagent. Reactions were incubated for 3 min at room temperature, added drop-wise to the well, and luciferase activity was assayed 18 h after transfection. Plasmid transfections were performed using Lipofectamine 2000 (Invitrogen), according to manufacturer's protocol, and Matrigel or western blot assays were performed 48 h post transfection. siRNA transfection was performed using Lipofectamine 2000, with the following modifications to manufacturer's protocol. 48 h after transfection, cells were split into new 6-well plates to be at ~70% confluence 24 h after seeding. These cells were then transfected for a second time with siRNA, and harvested for Matrigel or western blot assays 48 h post second transfection.

Plasmids and siRNAs

To generate the c-Jun and BTG1 5′ UTR luciferase reporter plasmids, sections of the 5′ UTR were first amplified from human cDNA. These were then stitched together downstream of a T7 promoter using overlap-extension PCR and Gibson cloning. For the PSMB6 5′ UTR luciferase reporter plasmid, the 5′ UTR was constructed by annealing primers together to create restriction site-compatible overhangs. The 5′ UTRs were then inserted together with Renilla luciferase into pUC19 for c-Jun and pcDNA4 for BTG1 and PSMB6. The eIF3 binding mutants and BTG1 stem loop chimeras were made by inserting annealed primers after cutting the plasmid with enzymes flanking the desired insertion site. The BTG1 overexpression plasmid was constructed by inserting the BTG1 open reading frame, isolated by PCR from human cDNA, into pcDNA4 modified with a Kozak site[30]. siRNA pools used were siGENOME Jun (Dharmacon M-003268-03) and siGENOME Non-Targeting siRNA #3 (Dharmacon D-001210-03).

Western blot

Western blot analysis was performed using the following antibodies: anti-eIF3a (Novus NBP1-18891); anti-eIF3b (Bethyl A301-761A); anti-eIF3c (Bethyl A300-376A); anti-eIF3d (Bethyl A301-758A); anti-eIF3e (Bethyl A302-985A); anti-eIF3f (Bethyl A303-005A); anti-eIF3g antibody (Bethyl A301-757A); anti-eIF3h antibody (Bethyl A301-754A); anti-eIF3i (Biolegend 646701); anti-eIF3k (Novus NB100-93304); anti-eIF3l antibody (Genetex GTX120119); anti-eIF3m (Novus NBP1-56654); anti-rpS19 (Bethyl A304-002A); anti-eIF4G1 (Bethyl A301-775A); anti-c-Jun (Bethyl A302-959A); anti-BTG1 (Abcam ab151740). anti-GAPDH (Bethyl A300-640A); anti-HSP90 (BD 610418).

In vitro transcription

RNAs were made by *in vitro* transcription with T7 RNA polymerase (NEB). For luciferase RNAs, transcription was performed in the presence of 3′-O-Me-m^{7}G(5′)ppp(5′)G RNA Cap Structure Analog (NEB), using linearized plasmid as the template, and poly-adenylated using polyA polymerase (Invitrogen). For gel shifts, annealed oligonucleotides were used as the template, and RNAs were radiolabeled by capping with vaccinia virus enzymes (NEB) and [α-^{32}P]-GTP. For SHAPE reactions, PCR templates were made using primers to add a

3′ handle (5′- GAACCGGACCGAAGCCCGGGCTGAG-3′), and transcription was performed using gel-extracted PCR products. RNAs were purified by phenol-chloroform extraction and ethanol precipitation or using the RNA Clean and Concentrator Kit (Zymo).

In vitro translation

In vitro translation extracts were made from 293T cells using a previously described protocol[31]. Briefly, cells were trypsinized and collected by centrifugation for 5 min at 1,000 × g at 4 °C. Cells were washed once with cold PBS (137 mM NaCl, 2.7 mM KCl, 100 mM Na_2HPO_4, 2 mM KH_2PO_4) and an equal volume of freshly made cold lysis buffer (10 mM HEPES-KOH pH 7.6, 10 mM KOAc, 0.5 mM $Mg(OAc)_2$, 5 mM DTT, and 1 Complete EDTA-free Proteinase Inhibitor Cocktail tablet (Roche) per 10 ml of buffer) was added. After hypotonic-induced swelling for 45 min on ice, cells were homogenized using a syringe attached to a 26G needle until ∼95% of cells burst, as monitored by trypan blue staining. Lysate was centrifuged at 14,000 × g for 1 min at 4 °C, and supernatant was moved to a new tube, avoiding the top lipid layer. Lysates were quickly frozen with liquid nitrogen and stored at −80 °C. Each translation reaction contained 50% *in vitro* translation lysate and buffer to make the final reaction with 0.84 mM ATP, 0.21 mM GTP, 21 mM creatine phosphate (Roche), 45 U ml^{-1} creatine phosphokinase (Roche), 10 mM HEPES-KOH pH 7.6, 2 mM DTT, 2 mM $Mg(OAc)_2$, 50 mM KOAc, 8 μM amino acids (Promega), 255 μM spermidine, and 1 U μl^{-1} murine RNase inhibitor (NEB). 1 mM $m^7G(5')ppp(5')G$ RNA cap structure analog (NEB) was added to reactions when indicated. Translation reactions were incubated for 1 h at 30 °C, after which luciferase activity was assayed.

eIF3 purification and native agarose gel electrophoresis

Recombinant eIF3 was expressed and purified from *E. coli* and native human eIF3 was purified from HeLa cells as previously described[32]. The gel shift protocol was adapted from [33] and [34]. A 0.7% agarose gel was prepared using Agarose Type 1B (Sigma A0576) in buffer consisting of 1× TBE supplemented with 75 mM KCl, and gel and buffer were pre-cooled at 4 °C. For each gel shift, 2 μl water, 1 μl of 5× Binding Buffer (25 mM Tris-HCl pH 7.5, 5 mM $Mg(OAc)_2$, 70 mM KCl, 0.1 mM $CaCl_2$, 0.1 mg ml^{-1} BSA, 2 mM TCEP), 1 μl labeled RNA, and 1 μl of purified eIF3 or protein buffer was added, in the listed order, and incubated at 25 °C for 30 min. 1 μl of room temperature 6× non-denaturing loading dye (40% w/v sucrose, with xylene cyanol and bromophenol blue) was added to the reactions and these were loaded on the agarose gel. The gel was run for 1 h at 40 V at 4 °C, buffer was replaced with fresh cold buffer, and the gel was run for another hour at 40 V. The gel was placed on top of positively charged nylon membrane with four pieces of Whatman filter paper underneath, covered in saran wrap, and dried for 1 h at 75 °C on a pre-heated gel drier. The gel was imaged using a phosphoimager.

SHAPE mapping of RNA structure

The SHAPE protocol was adapted from [35]. Each RNA folding reaction contained 1 μg of RNA, 1.8 μl 5× annealing buffer (100 mM HEPES-KOH pH 8.0, 50 mM KCl, 2.5 mM $MgCl_2$), and water to make the total reaction volume 9 μl. RNAs were incubated at 65 °C for 5 min, ice for 5 min, and then at 25 °C for 5 min. To each tube, 1 μl of 100% DMSO or 1

µl of 800 mM benzoyl cyanide (Sigma) was added, and the reaction was mixed by pipetting three times. The RNAs were immediately recovered by ethanol precipitation. Purified RNA was dissolved in 9 µl of 0.5× TE buffer (5 mM Tris, 0.5 mM EDTA pH 8.0). 3 µl of 0.3 µM NED- or VIC-labeled primers were added to the modified and unmodified reactions, respectively. For sequencing reactions, 1 µg of RNA in 1 µl volume was mixed with 8 µl of 0.5× TE buffer, and 3 µl of 0.3 µM FAM- or PET-labeled primers were added to each tube with 1 µl of 10 mM ddATP or ddTTP. To each tube, 7 µl of reverse transcription buffer (250 mM KCl, 167 mM Tris-HCl pH 8.3, 1.67 mM dNTPs, 17 mM DTT and 10 mM $MgCl_2$) was added and the reactions were pre-warmed to 52 °C for 1 min. 1 µl of Superscript III (Invitrogen) was added and the tubes were incubated at 52 °C for 50 min, 65 °C for 5 min, and then put on ice. The RNA was hydrolyzed by adding 0.5 µl 10 N NaOH, heating to 95 °C for 3 min, put on ice, and then neutralized by adding 0.33 µl of 12.1 M HCl. cDNAs were recovered by ethanol precipitation and resuspended in 11 µl of deionized formamide. Fragment analysis was performed using an Applied Biosystems 3730XL DNA Analyzer, and raw traces were analyzed using Shapefinder software[36].

Matrigel invasion assay

Matrigel assays were performed using Corning BioCoat Matrigel invasion chambers according to manufacturer's protocol. 24 h after seeding the invasion chambers, invaded cells were fixed with 70% ethanol and stained with crystal violet prior to imaging.

PAR-CLIP

Three biological replicates of PAR-CLIP were performed as previously described, with some modifications[5]. For each experiment, 40 to 50 150 mm plates of 293T cells were seeded to be at ∼90% confluence during crosslinking. 14 h prior to crosslinking, 4-thiouridine (Sigma) was added to the media to a final concentration of 100 µM. For crosslinking, the cells were washed with cold PBS and then the plates were irradiated on ice with 0.15 J cm^{-2} of UV 365 nm light. The cells were scraped into PBS, pelleted by centrifugation at 1,000 × g for 5 min at 4 °C, and the pellet was resuspended in three volumes of NP40 lysis buffer (50 mM HEPES-KOH pH 7.5, 150 mM KCl, 2 mM EDTA, 0.5% Nonidet P-40 alternative, 0.5 mM dithiothreitol (DTT), 1 Complete EDTA-free Proteinase Inhibitor Cocktail tablet per 50 ml of buffer). The cell suspension was incubated on ice for 10 min, passed through an 18G needle five times, and centrifuged at 13,000 × g for 15 min at 4 °C. The lysate was filtered through a 0.2 µm membrane syringe filter and RNAs were lightly digested by treatment with RNase T1 (Thermo Scientific) at a final concentration of 0.05 U $µl^{-1}$ for 15 min at room temperature. For each plate, 5 µl of Dynabeads (Invitrogen) and 10 µl of anti-eIF3b antibody (Bethyl A301-761A) were prepared by washing the beads once with PBS and 0.2% Tween-20, and then allowing the antibody to bind to the beads in PBS and 0.2% Tween-20 by rotating at room temperature for 15 min. The antibody and beads were added to the lysates and the immunoprecipitation was rotated at 4 °C for 2 h.

The beads were collected and washed three times in high salt NP40 wash buffer (50 mM HEPES-KOH pH 7.5, 500 mM KCl, 0.5% Nonidet P-40 alternative, 0.5 mM DTT, 1 Complete EDTA-free Proteinase Inhibitor Cocktail tablet per 50 ml of buffer). One bead

volume of NP40 lysis buffer and 50 U μl^{-1} RNase T1 was added to the beads and incubated for 16 min at room temperature. Beads were washed three times in high salt NP40 wash buffer and resuspended in one bead volume of Buffer 3 (NEB) with 0.5 U μl^{-1} Calf Intestinal Phosphatase (NEB). The reaction was incubated at 37 °C for 10 min, and beads were washed twice in phosphatase wash buffer (50 mM Tris-HCl pH 7.5, 20 mM EGTA, 0.5% v/v Nonidet P-40 alternative) and twice in PNK buffer without DTT (50 mM Tris-HCl pH 7.5, 50 mM NaCl, 10 mM $MgCl_2$). Beads were resuspended in one bead volume of PNK buffer with 0.5 μCi μl^{-1} [γ-^{32}P]-ATP and 1U μl^{-1} T4 PNK (NEB), and incubated for 20 min at 37 °C. 100 μM nonradioactive ATP was added and the reaction was incubated for 5 min at 37 °C, and then beads were washed five times with PNK buffer without DTT. SDS-PAGE loading dye (50 mM Tris-HCl pH 6.8, 100 mM β-Mercaptoethanol, 2% w/v SDS, 10% v/v glycerol, 0.1% bromophenol blue) was added to the beads, the sample was boiled for 5 min, and the sample was loaded onto a Bis-Tris 4-12% Bis-Tris gel (Novex) and electrophoresed in MOPS buffer (2.5 mM MOPS, 2.5 mM Tris base, 0.005% w/v SDS, 1 mM EDTA). As a size standard, native eIF3 was loaded onto the same gel.

The gel was imaged using a phosphoimager, a printed image was aligned to the gel, and the complexes were excised and electroeluted in a D Tube Dialyzer Midi (Millipore) for 2.5 h at 150 V, at 4 °C. The protein was digested with 1.2 mg ml^{-1} Proteinase K (Roche) in Proteinase K buffer (50 mM Tris-HCl pH 7.5, 75 mM NaCl, 6.25 mM EDTA, 1% w/v SDS) for 30 min at 37 °C. The RNA was isolated by phenol-chloroform extraction and ethanol precipitation, and small RNA libraries were prepared using a standard protocol[37]. The cDNA libraries were sequenced on an Illumina HiSeq 2000.

Mass spectrometry

Protein samples were prepared alongside the sequencing samples used for RNA library preparation, using five plates and substituting nonradioactive ATP during the T4 PNK labeling step. The samples were run on the same gel as the radiolabeled PAR-CLIP samples and cut out using the phosphorimager printout as a guide. Mass spectrometry samples were prepared by in-gel tryptic digestion[38] and peptides were identified by LC-MS.

Denaturing immunoprecipitation

The denaturing immunoprecipitation was performed using the PAR-CLIP protocol, with the following alterations. Five plates were used for each sample and, after crosslinking, one volume of NP40 lysis buffer was added and the sample was incubated on ice for 10 min. The lysate was clarified by centrifugation, the supernatant was transferred to a new tube, and one volume of 2 × SDS lysis buffer (10% w/v SDS, 100mM Tris-HCl pH 7.4, 10 mM EDTA, 20 mM DTT) was added. The sample was boiled for 5 min, cooled on ice, and then diluted at least ten fold with nondenaturing lysis buffer (1% v/v Triton-X 100, 50 mM HEPES-KOH pH 7.5, 150 mM NaCl, 2 mM EDTA). Immunoprecipitation was performed using an anti-eIF3d (Bethyl A301-758A) or anti-eIF3g (Bethyl A301-757A) antibody.

PAR-CLIP computational analysis

Raw Illumina reads were collapsed using fastx_collapser from FASTX Toolkit (http://hannonlab.cshl.edu/fastx_toolkit/), and 3′ adapters were removed using Cutadapt (http://

code.google.com/p/cutadapt/). Reads shorter than 15 nt were discarded. To remove processed reads that align to repeat elements, reads were mapped using Bowtie[39] to the hg19 RepeatMasker track from the UCSC table browser, and unmapped reads were retained. Retained reads were mapped to the hg19 reference genome, allowing for up to two mismatches in alignment. PARalyzer[10] was used to identify read clusters, or eIF3 crosslinking sites, with settings of five minimum read counts per group, cluster, or KDE, a minimum cluster size of 11 nt, and a minimum conversion count of 1. Clusters were annotated using iterative rounds of bedtools intersect[40], with the following hierarchy: start codon, stop codon, 5′ UTR, 3′ UTR, CDS, intron, lincRNA, miRNA, piwiRNA, snoRNA, snRNA, mitoRNA, rRNA, pseudogene, miscRNA. Annotation data was from the following sources: Gencode (v17 annotation) (http://www.gencodegenes.org), Ensembl BioMart, ncRNA database (http://www.ncrna.org/), miRBase (http://www.mirbase.org). Clusters that aligned to intergenic regions or that were antisense to the transcript were removed, along with any clusters that mapped identically but in the correct sense, as these are likely due to incorrect mapping[41]. Next, the consensus set of clusters was defined as a cluster that was reproduced in at least two of the three biological replicates[41], and this was determined using the Bioconductor GenomicFeatures package.

RNA-Seq

Two biological replicates of RNA-Seq were performed as following. Polyadenylated mRNAs were isolated from 5×10^6 293T cells using the mRNA-DIRECT kit (Ambion). For alkaline hydrolysis fragmentation, 250 ng of mRNA was mixed with 5× fragmentation buffer (150 mM $Mg(OAc)_2$, 200 mM Tris-Acetate pH 8.3, 500 mM KOAc) in a total volume of 20 μl and heated at 94 °C for 6 min. The RNA was ethanol precipitated, and first strand cDNA was synthesized using random hexamers and Superscript III (Invitrogen), according to manufacturer's protocol. For the following, the cDNA was purified between each step using a PCR purification column (Qiagen). To make second strand cDNA, 10 μl 10× ligase buffer (NEB), 0.3 mM dNTP mix, 67 U ml^{-1} *E. coli* DNA Ligase (NEB), 267 U ml^{-1} *E. coli* DNA, and 13.4 U ml^{-1} RNase H (Invitrogen) was added to the cDNA in a 100 μl reaction and incubated for 2.5 h at 16 °C. The cDNA was end repaired in a 100 μl reaction with 0.4 mM dNTPs, 10 μl 10× T4 DNA ligase buffer (NEB), 150 U ml^{-1} T4 DNA Polymerase (NEB), 50 U ml^{-1} T4 PNK (NEB), and 50 U ml^{-1} Klenow (NEB) for 30 min at 20 °C. To A-tail the cDNA, 2 mM dATP, 32 μl cDNA, 5 μl 10× NEBuffer 2 (NEB), and 300 U ml^{-1} Klenow exo (3′ to 5′ exo minus) (NEB) was added to the cDNA in a 50 μl reaction, and incubated for 30 min at 37 °C. To prepare adapters, 40 μM universal adapter and 40 μM indexed adapter were mixed with 2 μl 10× primer annealing buffer (100 mM Tris-HCl pH 8, 50 mM NaCl) in a 20 μl reaction and heated at 95 °C for 15 min, 70 °C for 15 min, and slow cooled to room temperature. Adapters were ligated in a 50 μl reaction with 5 μl 10× T4 DNA ligase buffer (NEB), 16000 U ml^{-1} T4 DNA ligase (NEB), and 2 μM adapters for 15 min at room temperature. cDNA libraries were amplified by PCR using Phusion (NEB) and 5 μM primer mix for 15 cycles of 10 s at 98 °C, 30 s at 65 °C, and 30 s at 72 °C, and isolated by gel purification (Qiagen). The cDNA libraries were sequenced using an Illumina HiSeq 2000. The following oligonucleotides were used: Universal adapter: 5′-AATGATACGGCGACCACCGAGATCTACACTCTTTCCCTACACGA CGCTCTTCCGATC*T-3′ (* denoting a phosphorothioate bond); Indexed adapter: 5′-/

5Phos/GATCGGAAGAGCACACGTCTGAACTCCAGTCAC-index-ATCTCGTATGCCGTC TTCTGCTTG-3′, with the index sequence being CGATGT or TGACCA); Primer mix: 5′-AATGATACGGCGACCACCGAGATCTACACTCTTTCCCTACACGA-3′ and 5′-CAAGCAGAAGACGGCATACGAGAT-3′.

RNA-Seq computational analysis

After quality filtering with the FASTX Toolkit, reads were mapped to the human hg19 genome using Tophat[42] and the Gencode (v17) annotation. FPKM was calculated using a python script, and the average FPKM was calculated using the two biological replicates.

RNA Immunoprecipitation and RT-PCR

Two 150 mm plates of 293T cells were lysed in three volumes of NP40 lysis buffer. Dynabeads were prepared with rabbit IgG (Cell Signaling 2729), rabbit anti-HA antibody (Invitrogen 71-5500), or rabbit anti-eIF3b antibody (Bethyl A301-761A). The lysate was split into three parts, the different antibody-Dynabead mixtures were added, and the suspension was incubated 2 h at 4 °C. The beads were washed four times with high NP40 wash buffer (50 mM HEPES-KOH pH 7.5, 500 mM KCl, 2 mM EDTA, 1% Nonidet P-40 alternative, 0.5 mM DTT), and bound RNAs were isolated by phenol-chloroform extraction and ethanol precipitation. cDNA was reverse transcribed using random hexamers and Superscript III, and PCR was performed using Phusion. The following oligonucleotides were used:

RANGAP1-Forward (5′-ACCGTCTGGAGAATGATGG-3′); RANGAP1-Reverse (5′-CGCAAGGTCTTCAAGGTCTC-3′); JUN-Forward (5′-TGACTGCAAAGATGGAAACG-3′); JUN-Reverse (5′-CCGTTGCTGGACTGGATTAT-3′); BTG1-Forward (5′-CACTGGTTCCCAGAAAAGC-3′); BTG1-Reverse (5′-CTACCATTTGCACGTTGGTG-3′); PPP3R1-Forward (5′-GAATTCATTGAGGGCGTCTC-3′); PPP3R1-Reverse (5′-GCCACCTACAACAGCACAGA-3′); CDK12-Forward (5′-CAAATTCTCAGCCCCCTGTA-3′); CDK12-Reverse (5′-GAGGTGGTGTGATTGCCTTT-3′); PSMB6-Forward (5′-ACTGGGAAAGCCGAGAAGTT-3′); PSMB6-Reverse (5′-TCCCGGTAGGTAGCATCAAC-3′).

Extended Data

Extended Data Figure 1. PAR-CLIP reveals eIF3a, b, d, and g bind to RNA

a, Mass spectrometry identification of trypsin-released peptides from RNA-crosslinked eIF3 subunits. Peptides identified by mass spectrometry are highlighted in pink. **b, c,** Crosslinking and denaturing immunoprecipitation to validate subunit identification. As eIF3d and g co-migrate with eIF3l and e/f, respectively, subunit identification was validated by immunoprecipitation of individual proteins after crosslinking and treatment of lysates with SDS treatment and boiling.

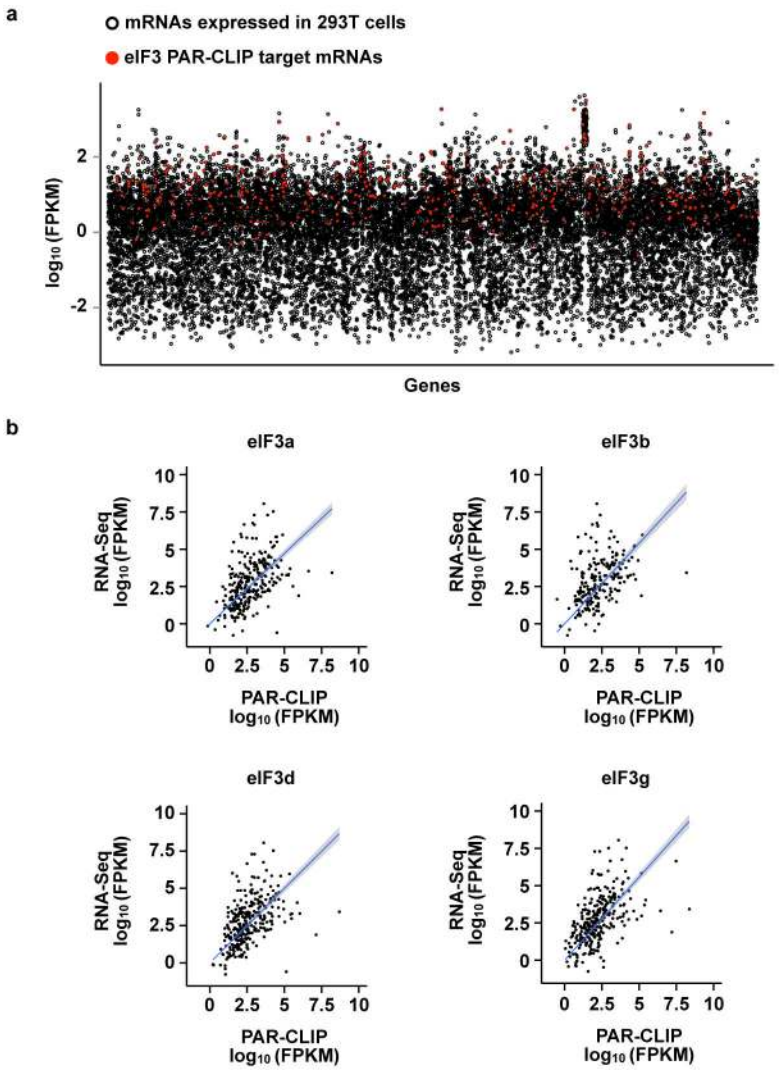

Extended Data Figure 2. Analysis of eIF3 PAR-CLIP targets

a, Scatterplot of fragments per kilobase of exon per million reads (FPKM) of all mRNAs expressed in 293T cells. mRNAs that are eIF3 PAR-CLIP targets are highlighted in red. **b,** Scatterplot of correlation between mRNA expression and PAR-CLIP read coverage for mRNAs that are eIF3 PAR-CLIP targets. The simple linear regression line is plotted in blue, with the 95% confidence region shaded in gray.

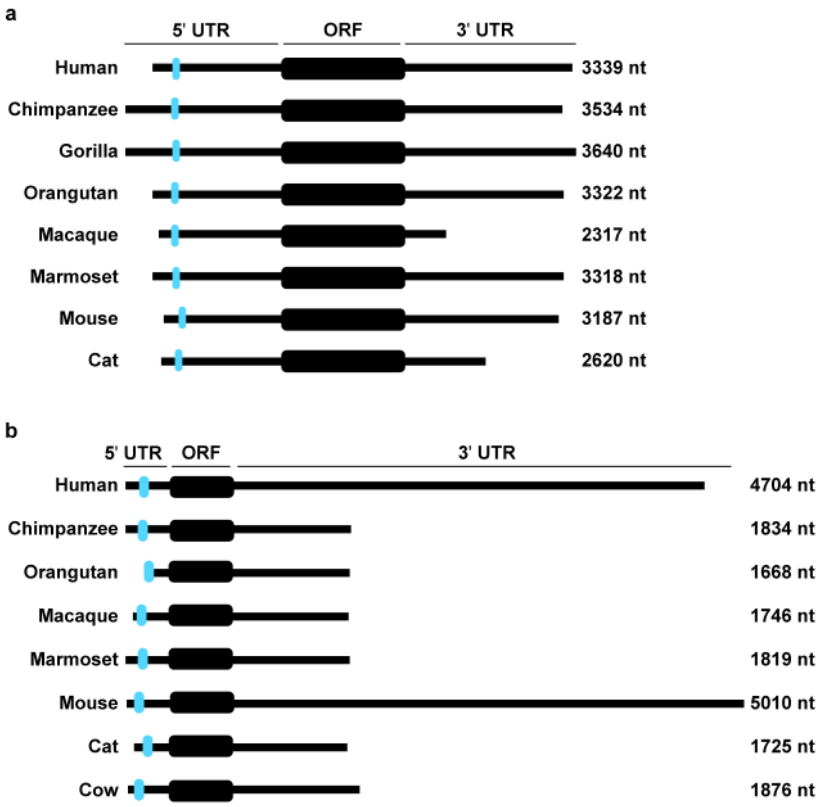

Extended Data Figure 3. Conservation of c-Jun and BTG1 eIF3-binding sites in primates and mammals

The eIF3-binding site is indicated in cyan. c-Jun Genbank IDs are: human (NM_002228.3, *Homo sapiens*), chimpanzee (XM_513442.5, *Pan troglodytes*), gorilla (XM_004025880.1, *Gorilla gorilla*), orangutan (XM_002810763.3, *Pongo abelii*), rhesus macaque (NM_001265850.2, *Macaca mulatta*), marmoset (XM_002750880.3, *Callithrix jacchus*), mouse (NM_010591.2, *Mus musculus*), cat (XM_006934825.1, *Felis catus*). BTG1 Genbank IDs are: human (NM_001731.2, *Homo sapiens*), chimpanzee (XM_509262.3, *Pan troglodytes*), orangutan (XM_002823578.2, *Pongo abelii*), rhesus macaque (NM_001266672.1, *Macaca mulatta*), marmoset (XM_002752814.3, *Callithrix jacchus*), mouse (NM_007569.2, *Mus musculus*), cat (XM_006933950.1, *Felis catus*), cow (NM_173999.3, *Bos taurus*).

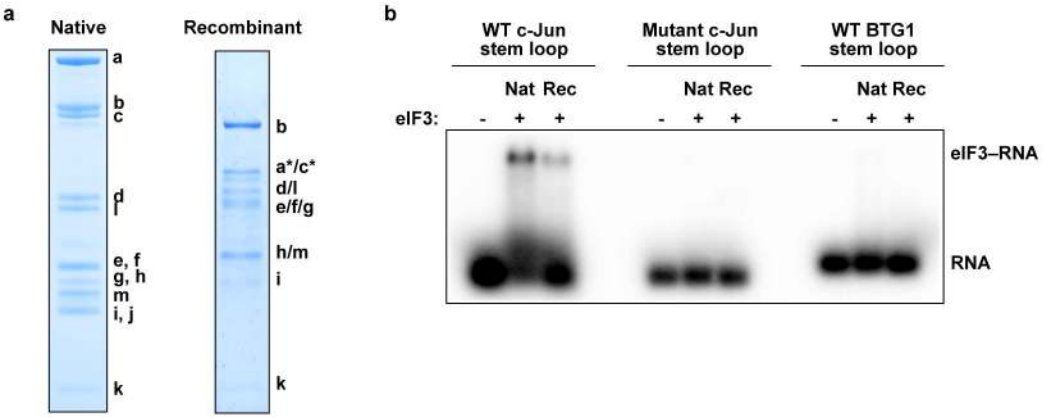

Extended Data Figure 4. Interactions between native and recombinant eIF3 and the c-Jun and BTG1 RNA stem loops

a, Coomassie blue staining of purified native HeLa eIF3 or recombinant eIF3, resolved by SDS-PAGE. **b**, Representative native agarose gel electrophoresis shows a specific and binary interaction between native and recombinant eIF3 and the WT Jun stem loop structure, but not with the mutated stem loop or the WT BTG1 stem loop.

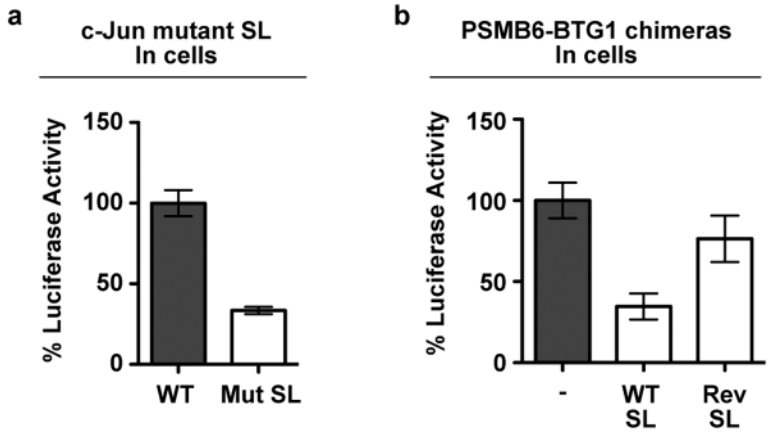

Extended Data Figure 5. Luciferase activity of c-Jun and BTG1 mutants in cells

a, b, Luciferase activity in 293T cells transfected with mRNAs containing the c-Jun 5′ UTR with a mutated stem loop (**a**) or the PSMB6 5′ UTR-BTG1 stem loop chimera (**b**). The results are given as the mean ± SD of three independent experiments, each performed in triplicate.

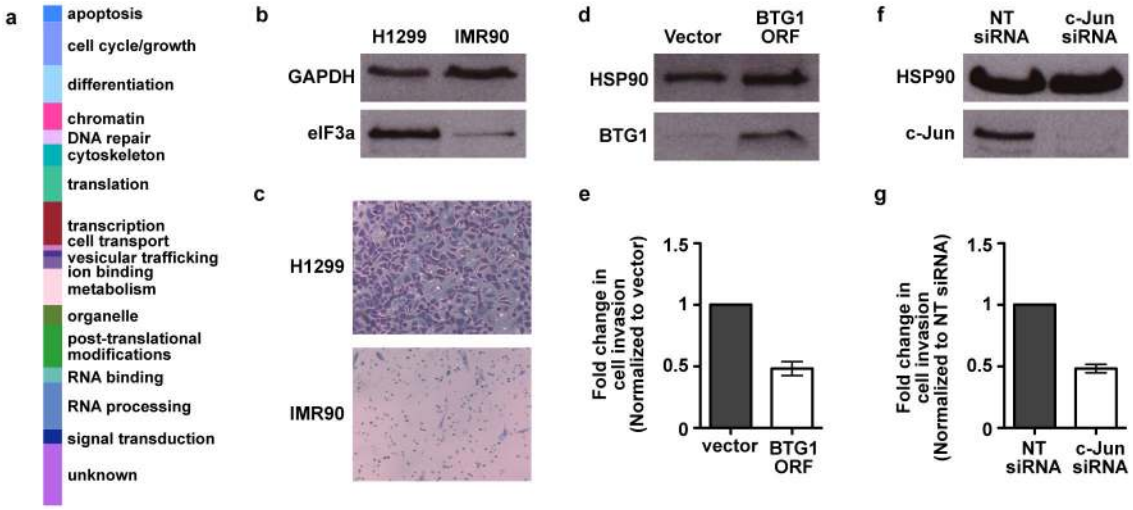

Extended Data Figure 6. Bypassing eIF3 translational control in H1299 cells reduces cell invasiveness

a, Functional classification of eIF3-bound RNAs. **b**, Representative western blot analysis of eIF3a expression levels in H1299 and IMR90 cells. GAPDH was detected as a loading control for normalized protein levels. **c**, Representative image of Matrigel invasion by H1299 or IMR90 cells. **d**, BTG1 protein levels after overexpression in H1299 cells. HSP90 was detected as a loading control. **e**, Matrigel invasion assay in H1299 cells after overexpression of BTG1. **f**, c-Jun protein levels after siRNA-mediated knockdown in H1299 cells. **g**, Matrigel invasion assay in H1299 cells after knockdown of c-Jun. The results of (**e**) and (**g**) are given as the mean ± SD of three independent experiments, each performed in duplicate.

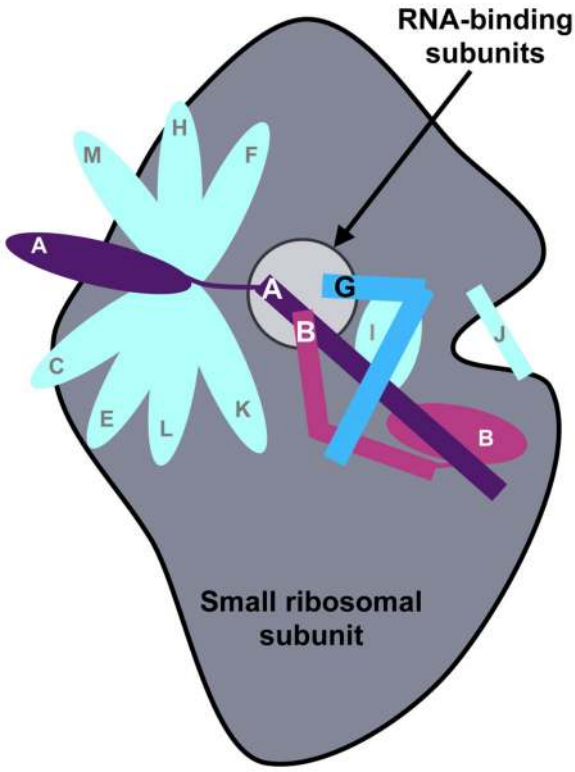

Extended Data Figure 7. Schematic of eIF3 subunits localization on the small ribosomal subunit

The eIF3 subunits bound to RNA in the PAR-CLIP experiment, eIF3a, b, and g, form a nexus in the distal eIF3 region. The location of eIF3d has not been assigned, and the schematic is adapted from [14].

Supplementary Material

Refer to Web version on PubMed Central for supplementary material.

Acknowledgments

The authors thank Jennifer Doudna, Davide Ruggero, Doug Black, Morgan Truitt, Akshay Tambe, Yun Bai, and Kozak Chat for helpful discussions. HeLa cytoplasm was a kind gift from Jie Fang. This work used the Vincent J. Coates Genomics Sequencing Laboratory at UC Berkeley, supported by NIH S10 Instrumentation Grants S10RR029668 and S10RR027303; and the Vincent J. Proteomics/Mass Spectrometry Laboratory at UC Berkeley, supported in part by NIH S10 Instrumentation Grant S10RR025622. This work was funded by the NIGMS Center for RNA Systems Biology (A.S.Y.L. and J.H.D.C.). A.S.Y.L is supported as an American Cancer Society Postdoctoral Fellow (PF-14-108-01-RMC) and P.J.K. is supported as an HHMI Fellow of the Life Sciences Research Foundation.

References

1. Stumpf CR, Ruggero D. The cancerous translation apparatus. Curr Opin Genet Dev. 2011; 21:474–483.10.1016/j.gde.2011.03.007 [PubMed: 21543223]
2. Silvera D, Formenti SC, Schneider RJ. Translational control in cancer. Nat Rev Cancer. 2010; 10:254–266.10.1038/nrc2824 [PubMed: 20332778]
3. Jackson RJ, Hellen CU, Pestova TV. The mechanism of eukaryotic translation initiation and principles of its regulation. Nat Rev Mol Cell Biol. 2010; 11:113–127.10.1038/nrm2838 [PubMed: 20094052]

4. Hershey JW. Regulation of protein synthesis and the role of eIF3 in cancer. Braz J Med Biol Res. 2010; 43:920–930. [PubMed: 20922269]
5. Hafner M, et al. Transcriptome-wide identification of RNA-binding protein and microRNA target sites by PAR-CLIP. Cell. 2010; 141:129–141.10.1016/j.cell.2010.03.009 [PubMed: 20371350]
6. Choudhuri A, Maitra U, Evans T. Translation initiation factor eIF3h targets specific transcripts to polysomes during embryogenesis. Proc Natl Acad Sci U S A. 2013; 110:9818–9823.10.1073/pnas.1302934110 [PubMed: 23716667]
7. Curran SP, Ruvkun G. Lifespan regulation by evolutionarily conserved genes essential for viability. PLoS Genet. 2007; 3:e56.10.1371/journal.pgen.0030056 [PubMed: 17411345]
8. Zhang L, Pan X, Hershey JW. Individual overexpression of five subunits of human translation initiation factor eIF3 promotes malignant transformation of immortal fibroblast cells. J Biol Chem. 2007; 282:5790–5800.10.1074/jbc.M606284200 [PubMed: 17170115]
9. Fraser CS, Doudna JA. Structural and mechanistic insights into hepatitis C viral translation initiation. Nat Rev Microbiol. 2007; 5:29–38.10.1038/nrmicro1558 [PubMed: 17128284]
10. Corcoran DL, et al. PARalyzer: definition of RNA binding sites from PAR-CLIP short-read sequence data. Genome Biol. 2011; 12:R79.10.1186/gb-2011-12-8-r79 [PubMed: 21851591]
11. Pisarev AV, Kolupaeva VG, Yusupov MM, Hellen CU, Pestova TV. Ribosomal position and contacts of mRNA in eukaryotic translation initiation complexes. EMBO J. 2008; 27:1609–1621.10.1038/emboj.2008.90 [PubMed: 18464793]
12. Hashem Y, et al. Structure of the mammalian ribosomal 43S preinitiation complex bound to the scanning factor DHX29. Cell. 2013; 153:1108–1119.10.1016/j.cell.2013.04.036 [PubMed: 23706745]
13. Hashem Y, et al. Hepatitis-C-virus-like internal ribosome entry sites displace eIF3 to gain access to the 40S subunit. Nature. 2013; 503:539–543.10.1038/nature12658 [PubMed: 24185006]
14. Erzberger JP, et al. Molecular Architecture of the 40SeIF1eIF3 Translation Initiation Complex. Cell. 2014; 158:1123–1135.10.1016/j.cell.2014.07.044 [PubMed: 25171412]
15. Wisdom R, Johnson RS, Moore C. c-Jun regulates cell cycle progression and apoptosis by distinct mechanisms. EMBO J. 1999; 18:188–197.10.1093/emboj/18.1.188 [PubMed: 9878062]
16. Rouault JP, et al. BTG1, a member of a new family of antiproliferative genes. EMBO J. 1992; 11:1663–1670. [PubMed: 1373383]
17. Bakker WJ, et al. FoxO3a regulates erythroid differentiation and induces BTG1, an activator of protein arginine methyl transferase 1. J Cell Biol. 2004; 164:175–184.10.1083/jcb.200307056 [PubMed: 14734530]
18. Blau L, et al. Aberrant expression of c-Jun in glioblastoma by internal ribosome entry site (IRES)-mediated translational activation. Proc Natl Acad Sci U S A. 2012; 109:E2875–2884.10.1073/pnas.1203659109 [PubMed: 23027969]
19. Kozak M. Circumstances and mechanisms of inhibition of translation by secondary structure in eucaryotic mRNAs. Mol Cell Biol. 1989; 9:5134–5142. [PubMed: 2601712]
20. Johnson R, Spiegelman B, Hanahan D, Wisdom R. Cellular transformation and malignancy induced by ras require c-jun. Mol Cell Biol. 1996; 16:4504–4511. [PubMed: 8754851]
21. Waanders E, et al. The origin and nature of tightly clustered BTG1 deletions in precursor B-cell acute lymphoblastic leukemia support a model of multiclonal evolution. PLoS Genet. 2012; 8:e1002533.10.1371/journal.pgen.1002533 [PubMed: 22359517]
22. Pincheira R, Chen Q, Zhang JT. Identification of a 170-kDa protein over-expressed in lung cancers. Br J Cancer. 2001; 84:1520–1527.10.1054/bjoc.2001.1828 [PubMed: 11384103]
23. Carlsten JO, Zhu X, Gustafsson CM. The multitalented Mediator complex. Trends Biochem Sci. 2013; 38:531–537.10.1016/j.tibs.2013.08.007 [PubMed: 24074826]
24. Andaya A, Villa N, Jia W, Fraser CS, Leary JA. Phosphorylation stoichiometries of human eukaryotic initiation factors. Int J Mol Sci. 2014; 15:11523–11538.10.3390/ijms150711523 [PubMed: 24979134]
25. Damoc E, et al. Structural characterization of the human eukaryotic initiation factor 3 protein complex by mass spectrometry. Mol Cell Proteomics. 2007; 6:1135–1146.10.1074/mcp.M600399-MCP200 [PubMed: 17322308]

26. Holz MK, Ballif BA, Gygi SP, Blenis J. mTOR and S6K1 mediate assembly of the translation preinitiation complex through dynamic protein interchange and ordered phosphorylation events. Cell. 2005; 123:569–580.10.1016/j.cell.2005.10.024 [PubMed: 16286006]
27. Kondrashov N, et al. Ribosome-mediated specificity in Hox mRNA translation and vertebrate tissue patterning. Cell. 2011; 145:383–397.10.1016/j.cell.2011.03.028 [PubMed: 21529712]
28. Lee AS, Burdeinick-Kerr R, Whelan SP. A ribosome-specialized translation initiation pathway is required for cap-dependent translation of vesicular stomatitis virus mRNAs. Proc Natl Acad Sci U S A. 2013; 110:324–329.10.1073/pnas.1216454109 [PubMed: 23169626]
29. Ule J, Jensen K, Mele A, Darnell RB. CLIP : a method for identifying protein-RNA interaction sites in living cells. Methods. 2005; 37:376–386.10.1016/j.ymeth.2005.07.018 [PubMed: 16314267]
30. Kranzusch PJ, et al. Structure-guided reprogramming of human cGAS dinucleotide linkage specificity. Cell. 2014; 158:1011–1021.10.1016/j.cell.2014.07.028 [PubMed: 25131990]
31. Rakotondrafara AM, Hentze MW. An efficient factor-depleted mammalian in vitro translation system. Nat Protoc. 2011; 6:563–571.10.1038/nprot.2011.314 [PubMed: 21527914]
32. Sun C, et al. Functional reconstitution of human eukaryotic translation initiation factor 3 (eIF3). Proc Natl Acad Sci U S A. 2011; 108:20473–20478.10.1073/pnas.1116821108 [PubMed: 22135459]
33. Davidovich C, Zheng L, Goodrich KJ, Cech TR. Promiscuous RNA binding by Polycomb repressive complex 2. Nat Struct Mol Biol. 2013; 20:1250–1257.10.1038/nsmb.2679 [PubMed: 24077223]
34. Kranzusch PJ, et al. Assembly of a functional Machupo virus polymerase complex. Proc Natl Acad Sci U S A. 2010; 107:20069–20074.10.1073/pnas.1007152107 [PubMed: 20978208]
35. Bai Y, Zhou K, Doudna JA. Hepatitis C virus 3′UTR regulates viral translation through direct interactions with the host translation machinery. Nucleic Acids Res. 2013; 41:7861–7874.10.1093/nar/gkt543 [PubMed: 23783572]
36. Vasa SM, Guex N, Wilkinson KA, Weeks KM, Giddings MC. ShapeFinder: a software system for high-throughput quantitative analysis of nucleic acid reactivity information resolved by capillary electrophoresis. RNA. 2008; 14:1979–1990.10.1261/rna.1166808 [PubMed: 18772246]
37. Hafner M, et al. Barcoded cDNA library preparation for small RNA profiling by next-generation sequencing. Methods. 2012; 58:164–170.10.1016/j.ymeth.2012.07.030 [PubMed: 22885844]
38. Shevchenko A, Tomas H, Havlis J, Olsen JV, Mann M. In-gel digestion for mass spectrometric characterization of proteins and proteomes. Nat Protoc. 2006; 1:2856–2860.10.1038/nprot.2006.468 [PubMed: 17406544]
39. Langmead B, Trapnell C, Pop M, Salzberg SL. Ultrafast and memory-efficient alignment of short DNA sequences to the human genome. Genome Biol. 2009; 10:R25.10.1186/gb-2009-10-3-r25 [PubMed: 19261174]
40. Quinlan AR, Hall IM. BEDTools : a flexible suite of utilities for comparing genomic features. Bioinformatics. 2010; 26:841–842.10.1093/bioinformatics/btq033 [PubMed: 20110278]
41. Lebedeva S, et al. Transcriptome-wide analysis of regulatory interactions of the RNA-binding protein HuR. Mol Cell. 2011; 43:340–352.10.1016/j.molcel.2011.06.008 [PubMed: 21723171]
42. Trapnell C, Pachter L, Salzberg SL. TopHat: discovering splice junctions with RNA-Seq. Bioinformatics. 2009; 25:1105–1111.10.1093/bioinformatics/btp120 [PubMed: 19289445]

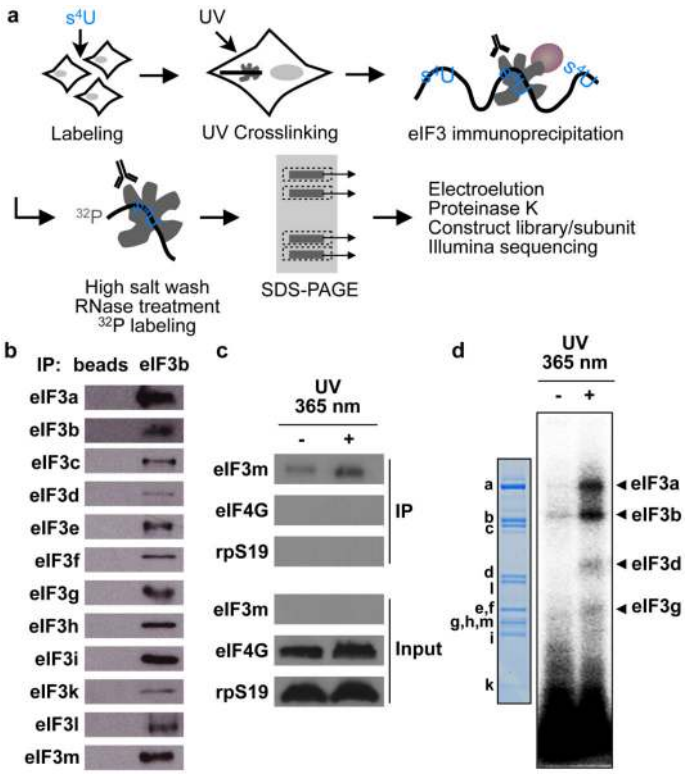

Figure 1. PAR-CLIP of the multi-protein translation initiation factor complex, eIF3

a, Schematic of PAR-CLIP methodology. 4-thiouridine-labeled (s^4U) RNAs were crosslinked to proteins and endogenous eIF3 complexes were immunoprecipitated using an antibody that recognizes eIF3b. Separate cDNA libraries were constructed for individual crosslinked subunits. **b,** Immunoprecipitation of the eIF3 complex. Magnetic beads without eIF3b antibody were used as a negative control. **c,** Western blot of immunoprecipitated complexes after PAR-CLIP. **d,** Phosphorimage of SDS gel resolving 5′ ^{32}P-labeled RNAs crosslinked to eIF3 subunits. Crosslinked RNAs cause the subunits to migrate ∼10 kD above their expected size[29]. Immunoprecipitated samples prepared from 4-thiouridine-labeled 293T lysates treated without UV 365 nm light are shown as a negative control. Coomassie blue staining of purified native eIF3 resolved by SDS-PAGE is shown for size reference.

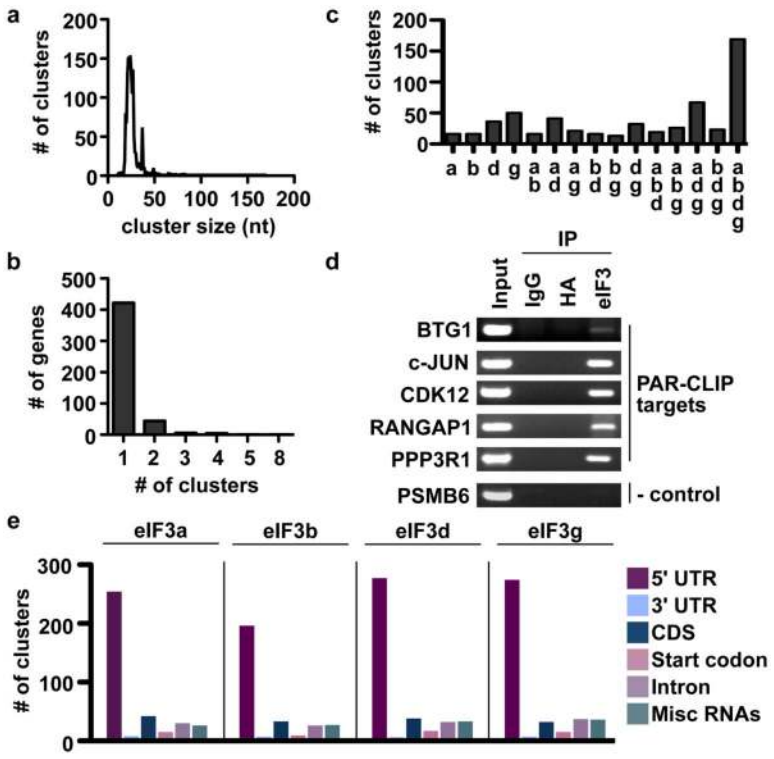

Figure 2. Analysis and validation of eIF3 PAR-CLIP-derived binding sites

a, Length distribution of PAR-CLIP clusters. **b,** Distribution of number of PAR-CLIP clusters per gene. **c,** Distribution of PAR-CLIP targets among different combinations of eIF3 subunit crosslinking. **d,** Validation of PAR-CLIP targets by eIF3 immunoprecipitation and RT-PCR. eIF3 immunoprecipitation was performed using an anti-eIF3b antibody as in Fig. 1b. As negative controls, the immunoprecipitation was performed with isotype-matched IgG or anti-HA antibody. **e,** Distribution of eIF3 crosslinking sites along mRNAs and in other classes of RNAs.

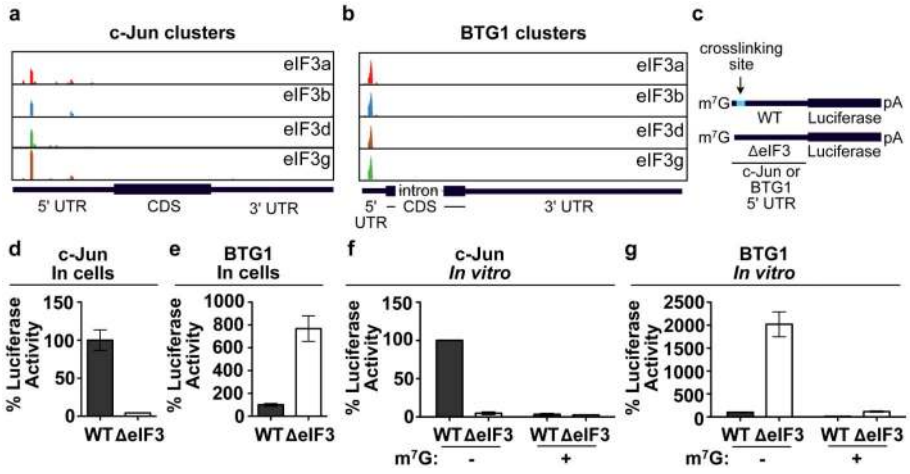

Figure 3. eIF3 is a positive and negative transcript-specific translational regulator

a, b, eIF3 PAR-CLIP cluster in the 5′ UTR of c-Jun mRNA (**a**) or BTG1 mRNA (**b**). Reads mapped are shown along the respective genes. **c,** Schematic of c-Jun and BTG1 5′ UTR-luciferase reporter mRNAs. The eIF3 PAR-CLIP cluster is nucleotide positions 181–214 for the c-Jun transcript (NM_002228) and positions 105–187 for the BTG1 transcript (NM_001731). **d, e,** Luciferase activity in cells transfected with mRNAs containing the c-Jun (**d**) or BTG1 (**e**) 5′ UTR with or without a deletion of the eIF3 crosslinking site. **f, g,** Luciferase activity *in vitro* from mRNAs driven by the c-Jun (**f**) or BTG1 (**g**) 5′ UTR, with or without competitor m^7G cap analog. The results of **d** – **g** are given as the mean ± SD of three independent experiments, each performed in triplicate.

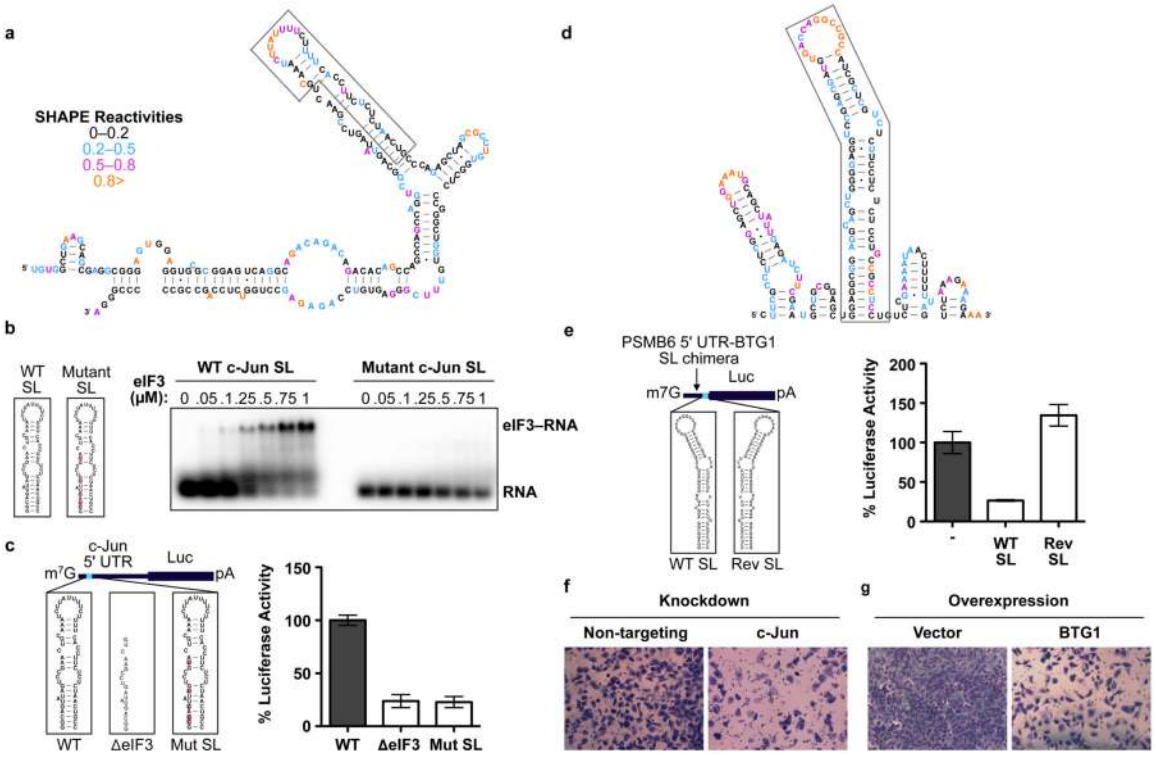

Figure 4. Opposing translation phenotypes are driven by different modes of eIF3–mRNA binding

a, SHAPE-based secondary structure of the c-Jun 5′ UTR surrounding the eIF3 PAR-CLIP site. Nucleotides are color-coded by their SHAPE reactivities, with higher reactivity reflecting single stranded behavior and non-reactivity indicating base pairing between nucleotides. **b,** Representative native gel shifts showing a specific and binary interaction between recombinant eIF3 and the wild type c-Jun stem loop structure but not the mutated stem loop. **c,** Luciferase activity *in vitro* of mRNAs driven by the c-Jun 5′ UTR containing stem loop mutations. **d,** SHAPE-based secondary structure of the BTG1 5′ UTR surrounding the eIF3 PAR-CLIP site. **e,** Luciferase activity *in vitro* from mRNAs driven by a PSMB6 5′ UTR-BTG1 stem loop chimera. The results of **c** and **e** are given as the mean ± SD of three independent experiments, each performed in triplicate. **f, g,** Representative images of the effect of siRNA-mediated knockdown of c-Jun (**f**) or BTG1 overexpression (**g**) on Matrigel invasion by H1299 cells. As a control, cells were transfected with a non-targeting siRNA (**f**) or empty vector (**g**). Quantification of cell migration is presented in Extended Data Fig. 6.